Light-Scattering-Studies of Dynamical Processes in Disparate Mass Gas-Mixtures

Wegdam, G.H.; Schaink, H.M.

DOI
10.1103/PhysRevA.40.7301

Publication date
1989

Published in
Physical Review A. General Physics

Light-scattering studies of dynamical processes in disparate mass gas mixtures

G. H. Wegdam and H. M. Schaink
Laboratory for Physical Chemistry, University of Amsterdam, Nieuwe Achtergracht 127, 1018 WS Amsterdam, The Netherlands
(Received 15 August 1989)

Results of light-scattering experiments on helium and xenon gas mixtures are presented for a large range of wave vectors, densities, and compositions. In the experiments these variables are varied independently from each other. In this manner we are able to show that the hydrodynamic eigenfrequencies, reduced with respect to the product of the wave vector k and the adiabatic sound velocity c_s, are a function of the product of the wave vector and the mean free path l_{He} only. By comparing the experimentally obtained dispersion curves and the predictions of the hydrodynamic theory, we find that the value of kl_{He} at which the theory ceases to be valid is independent of the composition. We show that the longitudinal current-current correlation function $\omega^2 I(k,\omega)$ is a useful function in the study of light-scattering spectra that are featureless. For large reduced wave vectors we find a sound mode that is solely supported by the fluctuations in the xenon density. This is the slow sound mode.

I. INTRODUCTION

Light-scattering as well as neutron-scattering experiments have contributed much to our understanding of the dynamical properties of matter.[1,2] Both experimental techniques yield information about the wave-vector and frequency dependence of the dynamic structure factor $S(k,\omega)$. However, the wave vectors k that are accessible in neutron scattering are typically three orders of magnitude larger than those that are probed in light-scattering experiments. Therefore the results obtained in these experiments complement each other. In the study of the condensed phase light scattering can be used to obtain several macroscopic properties [the small wave-vector limit of $S(k,\omega)$].[1,3] Neutron scattering yields information about the manner on which $S(k,\omega)$ passes over from the hydrodynamic regime ($k\sigma<2\pi$; σ represents the hard-sphere radius of the particles) to the kinetic regime ($k\sigma>2\pi$).[4] On the other hand, in gases a similar changeover between these two wave-vector regimes can be found when the product of the wave vector and the mean free path approaches unity. This wave-vector regime is accessible by light scattering provided that a proper choice of the thermodynamic circumstances is made.[5,6] In this paper we will study the wave-vector and density dependence of the light-scattering spectrum of binary gas mixtures. The relationship of the light-scattering spectrum $I(k,\omega)$ of a binary mixture and the partial dynamic structure factors is given by

$$I(k,\omega)\cong\alpha_1^2 x_1 S_{11}(k,\omega)+2\alpha_1\alpha_2\sqrt{(x_1x_2)}S_{12}(k,\omega)+\alpha_2^2 x_2 S_{22}(k,\omega)\ . \tag{1.1}$$

Here α_i and x_i represent the polarizability and the mole fraction of component i, respectively. In Eq. (1.1) we have neglected the influence of temperature fluctuations.

The molecular dynamics of a binary gas mixture is, to a large extent, determined by the mass ratio m_1/m_2 of the components, which—according to simple kinetic theory—causes a difference in the thermal velocities v_i of the particles: $v_1/v_2=\sqrt{(m_2/m_1)}$. On a macroscopic scale the effect of a large difference in mass is a strong correlation between concentration fluctuations and fluctuations in the pressure and the entropy. This correlation will affect the line shape of the Rayleigh-Brillouin spectrum, even at wave vectors for which the small wave-vector limit of the hydrodynamic theory is valid.[6]

Most of the light-scattering experiments on binary gas mixtures that have been performed up to this moment[5,7–10] followed the same procedure. Spectra were measured of successive gas mixtures that were prepared by adding helium to a fixed quantity of a heavier inert gas, thereby changing, simultaneously, concentration and density. The scattering angle remained fixed during these experiments. Up to this moment, not much attention has been paid to the measurement of dispersion relations. Baharudin *et al.*[11] have published the wave-vector dependence of the Brillouin lines for the He+Kr gas mixture ($m_{\mathrm{Kr}}/m_{\mathrm{He}}\cong 20$) with a krypton mole fraction $x_{\mathrm{Kr}}=0.8$, and they have shown that the Brillouin shift can be described by the simplified hydrodynamic model of Gornall and Wang[10] and Lekkerkerker and Boon.[12] A nonlinear dispersion curve is established by us experimentally in a He+Xe gas mixture, and we have shown that the curvature of the dispersion relation depends on the density.[13]

In a recent publication[6] we have studied extensively the wave-vector dependence of the eigenmodes of the hydrodynamic matrix for binary gas mixtures. We have found that deviations from the linear dispersion relation $z_s''=c_s k$ become more pronounced as the mass ratio of the components becomes larger. Especially in the case of the He+Xe gas mixture the hydrodynamic theory predicts that the dispersion relation may exhibit a local minimum at $k\neq 0$ for $x_{\mathrm{Xe}}<0.45$, while for $x_{\mathrm{Xe}}<0.16$ for certain wave vectors the sound wave may even cease to

propagate. These features of the dispersion relation occur for wave vectors $k\sigma = O(0.001)$. This contrasts with the dispersion relations which are observed in a great variety of systems in the condensed phase,[14–17] where a dip in the dispersion curve is found at $k\sigma \cong 2\pi$. We expect that the nonlinearity of the dispersion relations is related with the onset of the change from the hydrodynamic regime to the kinetic regime.

Another intriguing phenomenon that has been found recently in disparate mass mixtures is the occurrence of a fast sound wave supported by the light particles.[18,19] The first evidence of this behavior was found in a molecular-dynamics simulation of the Pb+Li mixture ($m_{\mathrm{Pb}}/m_{\mathrm{Li}} \cong 30$).[18] Recently, a fast sound mode has been measured by Montfrooij *et al.*[20] in a liquid He+Ne mixture using neutron scattering.

In this paper we will present experimental data concerning nonlinear dispersion relations in He+Xe gas mixtures. Our aim is to establish the deviations from the linear dispersion relation $z_s'' = c_s k$, and to investigate whether for intermediate and "large" wave vectors evidence can be found of a sound wave which is supported by only one species of particles. We will also test the prediction of the hydrodynamic theory that the eigenfrequencies z of the hydrodynamic matrix reduced with respect to $c_s k$ are a function of the quotient of the wave vector and the density.[6] Finally, we will make an assessment about the range of wave vectors for which the hydrodynamic theory is valid. To achieve our goal we perform our experiments and data analysis in a way which differs from most of the previous studies of similar systems.[5,7–10] In our case it is essential that we measure light-scattering spectra $I(k,\omega)$ as function of the wave vector or the density without varying simultaneously the composition of the mixtures. Also, rather than an overall line shape analysis, we will focus our attention to the wave-vector (or density) dependence of several features of $I(k,\omega)$.

II. THEORY

The frequency distribution of the scattered light is determined by the time dependence of the fluctuations of the dielectric constant $\delta\epsilon$:

$$I(k,\omega) = \int dt\, e^{i\omega t} I(k,t) \propto \int dt\, e^{i\omega t} \langle \delta\epsilon(k,0)\delta\epsilon(-k,t)\rangle \ . \tag{2.1}$$

The wave vector of the fluctuations that are probed is determined by the scattering geometry:

$$k = \frac{4\pi n}{\lambda} \sin\frac{\theta}{2} \ , \tag{2.2}$$

where λ, n, and θ stand for the wavelength of the incident light, the refractive index of the medium, and the scattering angle, respectively.

First we consider $I(k,\omega)$ in the limit of small wave vectors. For gas mixtures, "small" is used in the sense of being small compared to the reciprocal of the mean free path. Then the line shape can be described as a sum of Lorentzians, one for each eigenmode. For one-component fluids the Rayleigh line is given by a single Lorentzian (the thermal mode). In the case of binary mixtures, a second Lorentzian, which is due to the concentration fluctuations, is needed for the theoretical description of the Rayleigh line.[1,21] The sound modes give rise to the Brillouin lines. The resulting expression for the Rayleigh-Brillouin triplet is

$$\pi I(k,\omega) = A_D + \frac{z_{D+}}{z_{D+}^2 + \omega^2} + A_{D-}\frac{z_{D-}}{z_{D-}^2 + \omega^2} + [A_{s\pm}' z_s' \pm A_{s\pm}''(\omega \pm z_s'')]\frac{1}{(z_s')^2 + (\omega \pm z_s'')^2} \ . \tag{2.3}$$

Here $z_{D\pm}$ and $z_{s\pm} = z_s' \pm i z_s''$ represent the eigenfrequencies corresponding to the diffusive and propagating eigenmodes of the hydrodynamic matrix. Using perturbation theory one finds in the limit of very small wave vectors[21]

$$z_{D\pm} = \tfrac{1}{2}\{(D_T + \mathcal{W}D) \pm [(D_T - \mathcal{W}D)^2 + 4(\mathcal{W}-1)DD_T]^{1/2}\}k^2 \ , \tag{2.4}$$

$$z_{s\pm} = \pm i c_s k + \tfrac{1}{2}\left[D_v + (\gamma - 1)D_T + c_s^2 \rho^2 \left(\frac{\partial c}{\partial \mu}\right)_{p,T} \mathcal{P}^2 D\right] k^2 \ ,$$

with

$$\mathcal{W} = \frac{k_T^2}{T c_p}\left(\frac{\partial \mu}{\partial c}\right)_{p,T} + 1 \ , \qquad \mathcal{P} = -\frac{1}{\rho^2}\left(\frac{\partial \rho}{\partial c}\right)_{p,T}\left(\frac{\partial c}{\partial \mu}\right)_{p,T} + \frac{k_T \alpha_T}{\rho c_p} \ . \tag{2.5}$$

The quantities in these equations are the following: D is the binary diffusion constant, D_v the kinematic viscosity, D_T the thermal diffusivity, k_T the thermal diffusion ratio, p the pressure, ρ the mass density, c the mass concentration of the light component (in our case helium), T the temperature, c_s the adiabatic sound velocity, c_p the heat capacity per unit mass, α_T the thermal expansion coefficient, and $\mu = (\mu_1/m_1 - \mu_2/m_2)$ difference in the chemical potential per unit mass of the two components.

The light-scattering spectrum will become featureless as the wave vector changes from small to large values. This may make the interpretation of $I(k,\omega)$ troublesome. However, the function $\omega^2 I(k,\omega)$ has well-defined peaks for all wave vectors, even in the intermediate wave-vector region where the hydrodynamic theory predicts sound-propagation gaps.[6] It should be noted that $\omega^2 I(k,\omega)$ is closely related to the longitudinal current-current autocorrelation function.[2] For the peak positions $\omega_m(k)$ of $\omega^2 I(k,\omega)$ analytic expressions are known for both the small and large wave-vector limits.[14(b),22] In the small wave-vector limit it is possible to represent $\omega^2 I(k,\omega)$ as a combination of Lorentzians, similar to Eq. (2.3):

$$\pi\omega^2 I(k,\omega) = -A_{D+}z_D^2 + \frac{z_{D+}}{z_{D+}^2+\omega^2} - A_{D-}z_D^2 - \frac{z_{D-}}{z_{D-}^2+\omega^2} - [B_s' z_s' \pm B_s''(\omega \pm z_s'')]\frac{1}{(z_s')^2+(\omega\pm z_s'')^2} , \tag{2.6}$$

with

$$B_s' = A_s'(z_s'^2 - z_s''^2) - 2A_s'' z_s' z_s'' ,$$
$$B_s'' = A_s''(z_s'^2 - z_s''^2) + 2A_s' z_s' z_s'' .$$

In the small wave-vector limit we find that the peak positions of $\omega^2 I(k,\omega)$ are located at the same frequency as the Brillouin lines: $\omega_m(k) = z_s'' = c_s k$. Since $\omega^2 I(k,\omega)$ has well-defined peaks for every wave vector, it can be a useful tool in our attempt to study the deviations from the small wave-vector limit of the hydrodynamic theory.

In the limit of very large wave vectors the motion of individual particles is monitored by the light-scattering experiment. Then, due to the Doppler broadening by the Maxwellian velocity distributions of the different particles, the frequency spectrum is no longer a Rayleigh-Brillouin triplet, but a combination of Gaussians located at $\omega = 0$.[1,2]

$$I(k,\omega) \propto \sum_i \frac{x_i (\partial\epsilon/\partial n_i)^2_{n_{j\neq i},T}}{\sqrt{2\pi} k v_i} \exp[-\tfrac{1}{2}(\omega/kv_i)^2] , \tag{2.7}$$

with $i = \mathrm{Xe}, \mathrm{He}$, and n_i and $v_i = \sqrt{(k_B T/m_i)}$ representing the number density and the thermal velocity of species i, respectively. For the helium-xenon mixtures considered here

$$x_{\mathrm{Xe}} (\partial\epsilon/\partial n_{\mathrm{Xe}})^2_{n_{\mathrm{He}},T}/v_{\mathrm{Xe}} \gg x_{\mathrm{He}} (\partial\epsilon/\partial n_{\mathrm{He}})^2_{n_{\mathrm{Xe}},T}/v_{\mathrm{He}} \tag{2.8}$$

(polarizability ratio is $\alpha_{\mathrm{Xe}}/\alpha_{\mathrm{He}} \cong 20$;[23] $v_{\mathrm{Xe}}/v_{\mathrm{He}} \cong \frac{1}{6}$). Thus we find that in the large wave-vector limit $I(k,\omega)$ can be properly represented by a single Gaussian which described the free flight of a xenon particle. In this Gaussian limit it is easy to show that the peak positions of $\omega^2 I(k,\omega)$ are located at $\omega_m(k) = v_{\mathrm{Xe}} k\sqrt{2}$.[14(b)]

One of our aims is to establish the wave-vector regime in which the hydrodynamic theory is valid. In order to perform this task we will compare our experimental results with the predictions of the hydrodynamic theory formulated by Cohen *et al.*[21] Therefore we will analyze our experiments using Eq. (2.3), as well as determine the peak positions of $\omega^2 I(k,\omega)$. In this paper we will focus our attention especially on the wave-vector dependence of the sound mode. The calculation the wave-vector and density dependence of the eigenfrequencies of the hydrodynamic matrix which correspond to the sound mode, is similar to the calculations we published earlier.[6,22]

We will present the results of the data analysis as a function of the reduced wave vector kl_{He}, where l_{He} represents the mean free path of a helium particle:[6]

$$l_{\mathrm{He}} = \{\pi n [x_{\mathrm{Xe}} \sigma^2_{\mathrm{Xe\,He}} (m_{\mathrm{He}}/m_{\mathrm{red}})^{1/2} + \sqrt{2} x_{\mathrm{He}} \sigma^2_{\mathrm{He}}]\}^{-1} . \tag{2.9}$$

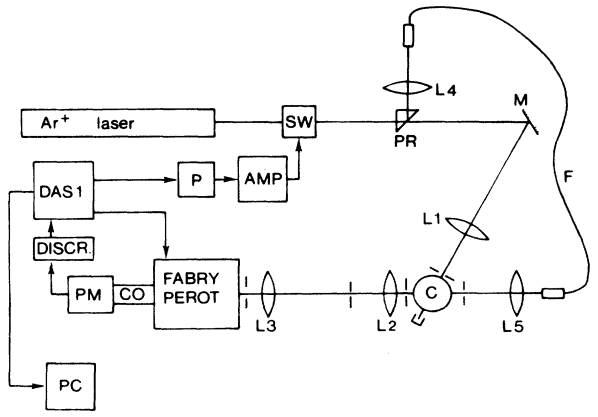

FIG. 1. The experimental setup, as used for the density-dependent measurements (with an exception of series 5a). Abbreviations used: L, lens; M, mirror; PR, prism; F, fiber; C, sample cell; CO, collimator; PM, photomultiplier; DISCR, amplifier and discriminator; P, pulse generator; AMP, amplifier; SW, acousto-optical switch; PC, computer.

Here, $\sigma_{\mathrm{Xe}} = 0.3963$nm, $\sigma_{\mathrm{He}} = 0.263$ nm (Ref. 24), and $\sigma_{\mathrm{Xe\,He}} = (\sigma_{\mathrm{Xe}} + \sigma_{\mathrm{He}})/2$, while n denotes the number density and m_{red} the reduced mass: $m_{\mathrm{red}} = m_{\mathrm{Xe}} m_{\mathrm{He}}/(m_{\mathrm{Xe}} + m_{\mathrm{He}})$. By presenting the eigenvalues of the hydrodynamic matrix, which are related to the observed widths and shifts of the light-scattering spectrum, as a function of kl_{He}, the main density dependence of these quantities is given by the product kl_{He}. It is easy to show that kl_{He} has only a slight composition dependence, so it is a straightforward matter to compare the results obtained for different compositions. We will show here that this definition of the reduced wave vector yields a simple condition for the validity of hydrodynamics.

III. EXPERIMENT

In Fig. 1 a sketch of the light-scattering setup is given. An argon-ion laser, operating single mode at 514.5 nm and with an output of 250 mW, is used as a light source. A vertically polarized laser beam is focused by lens L1 into the center of the cell. The scattering angle θ is determined by the location of mirror M1, and can be calculated using trigonometric relations. The scattered radiation is direction to a Fabry-Perot interferometer. The spectra

TABLE I. A review of the mixtures we have studied. In our experiments we have varied either the wave vector k or the total pressure p.

x_{Xe}	Initial total pressure (bar)	Variable parameter	Plate separation (cm)
0.53±0.02	41.8	p	4.60
0.53±0.02	9.9	k	4.60
0.79	41.3	p	9.0
0.61	38.3	p	6.49
0.45	37.8	p	3.49
0.38	35.2	p	3.49
0.22	38.7	p	3.49

are measured with a Burleigh RC-110 Fabry-Perot or a homemade version. Both interferometers are equipped with flat plates, and can be scanned piezoelectrically. The linearity of the scanned frequency versus time is better than 2%. The plate separation is measured with calipers; the free spectrum range of all the experiments is given in Table I. Data are collected in a Burleigh Das-1 data acquisition-stabilization system, which also maintained the interferometer alignment. We have measured the light-scattering spectra simlutaneously with the instrumental profile of the interferometer. This is done with the aid of an acousto-optical switch which is triggered by the acquisition unit. The switch produced a light pulse which is led to a position on the optical axis of the interferometer by means of a glass fiber. In this manner we measured interferograms which in the first order contained the instrumental profile and in the second and third order a spectrum of the light scattered by the sample.

In our experiments we have chosen the plate separation of the Fabry-Perot interferometer in such a manner that the shift of the Brillouin lines with respect to the Rayleigh line is always smaller than $\frac{1}{3}$ of the free spectral range between two successive orders. The plate separations are given in Table I. The free spectral range can be calculated with $\Delta\omega_{\mathrm{FSR}}=\pi c/d$, where c and d represent the velocity of light and the plate separation, respectively. The finesse has a typical value of $\Delta\omega_{\mathrm{FSR}}/\Delta\omega_{\mathrm{FWHM}}\cong 50$, or better.

The wave-vector-dependent measurements are performed using a scattering cell which consists of a carefully polished quartz cylinder that can be moved by translation stages in all three directions. For the density-dependent measurements we have used a sample cell which was designed for a 90° scattering geometry. A more detailed description of the sample cells is given elsewhere.[22] Both cells are connected to a gas handling system and a pressure gauge.

The experiments are performed at room temperature ($T=294$ K).

In our experiments high-grade gases are used, obtained from Air Products and Messer Griesheim. The gas mixtures are made using the following procedure. First, the sample cell is filled with xenon up to a pressure p_{Xe} and then helium is added up to a total pressure $p_{\mathrm{tot}}\cong 40$ bar. The mixture is allowed to equilibrate for a few days. Using an equation of state up to the third virial coefficient, we have calculated the density and the composition of the mixture, as well as the thermodynamic quantities needed for the hydrodynamic description. Details of these calculations are given elsewhere.[6,13,22]

IV. DATA ANALYSIS AND RESULTS

In Fig. 2 we show several Rayleigh-Brillouin spectra of two series with different compositions: $x_{\mathrm{Xe}}=0.45$ and $x_{\mathrm{Xe}}=0.22$. It can be seen from Fig. 2 that the spectral features become less distinct as the reduced wave vector increases (the density is lowered). For the mixture with $x_{\mathrm{Xe}}=0.45$ the Brillouin lines can be distinguished for all reduced wave vectors considered here ($kl_{\mathrm{He}}<0.8$). This is also the case for mixtures with a higher xenon concen-

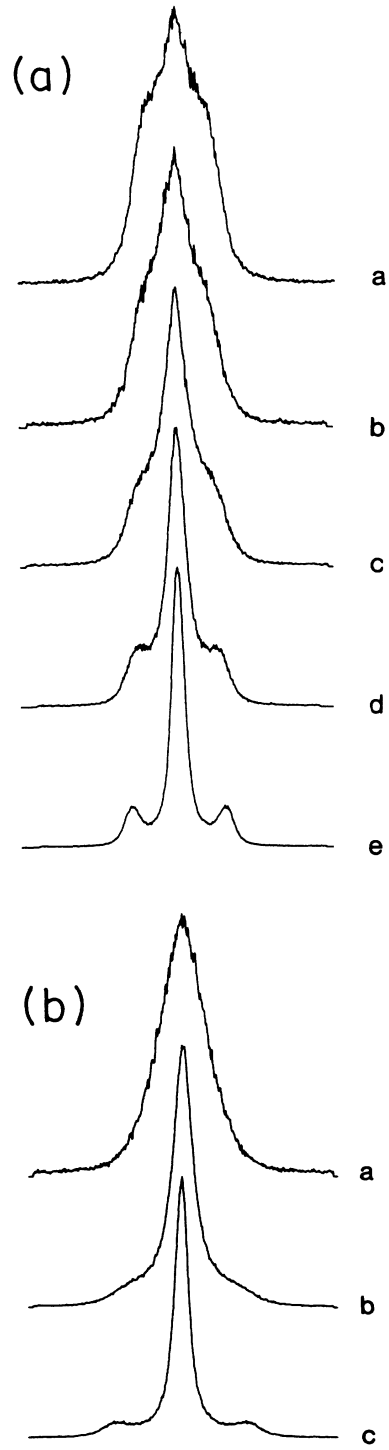

FIG. 2. (a) Several experimental Rayleigh-Brillouin spectra as a function of the density. Thermodynamic circumstances: $T=294$ K, $x_{\mathrm{Xe}}=0.45$. Curve a: $p=2.8$ bar, $kl_{\mathrm{He}}=0.77$; curve b, $p=5.6$ bar, $kl_{\mathrm{He}}=0.64$; Curve c, $p=9.0$ bar, $kl_{\mathrm{He}}=0.24$; curve d, $p=17.4$ bar, $kl_{\mathrm{He}}=0.12$; curve e, $p=37.8$ bar, $kl_{\mathrm{He}}=0.06$. (b) Several experimental Rayleigh-Brillouin spectra as a function of the density. Thermodynamic circumstances: $T=294$ K, $x_{\mathrm{Xe}}=0.22$; Curve a, $p=6.4$ bar, $kl_{\mathrm{He}}=0.35$; curve b, $p=18.3$ bar, $kl_{\mathrm{He}}=0.12$; curve c, $p=38.7$ bar, $kl_{\mathrm{He}}=0.06$.

tration. In this respect, a difference is obtained regarding the kl_{He} dependence of the light-scattering spectra measured on the mixture with $x_{Xe}=0.22$. The light-scattering spectra of the ($x_{Xe}=0.22$) mixture become featureless when kl_{He} exceeds 0.15.

An experimentally obtained light-scattering spectrum is a convolution of the instrumental profile of the experimental setup, and a line shape due to the processes which are probed:

$$I_{expt}(k,\omega)=I_{instr}(\omega)\circ I(k,\omega) . \quad (4.1)$$

In order to extract the values of z_i from our experiments, we have used the following procedure. We have approximated $I(k,\omega)$ as a sum of three Lorentzians and $I_{expt}(k,\omega)$ was calculated by convoluting $I(k,\omega)$ with the simultaneously measured instrumental profile. The χ^2 merit function of the experimental line shape and the calculated $I_{expt}(k,\omega)$ is minimalized with a simplex routine. These results served as input for a second fitting procedure in which the asymmetric contribution to the Brillouin lines is included. The amplitude of the asymmetric contribution is calculated using the sum rule[14(a)]

$$2z_s'' A_s''=z_D A_D+2z_s' A_s' . \quad (4.2)$$

In Eq. (4.2) A_D, A_s', and A_s'' represent the amplitudes of the Rayleigh line, Brillouin lines, and the asymmetric contribution, while z_D, z_s', and z_s'' represent the width of the Rayleigh line, the attenuation factor, and the propagation frequency of the sound mode, respectively [see also Eq. (2.3)]. Throughout the fitting procedure, we have assumed that the Rayleigh line can be described by a single Lorentzian. One may question this ansatz. However, on the basis of our calculations[6] we can conclude that the Rayleigh line is always dominated by one of the two possible diffusive modes ($D+$ and $D-$), for almost all wave vectors. In the small wave-vector region where the amplitudes of both the diffusive modes are of the same order

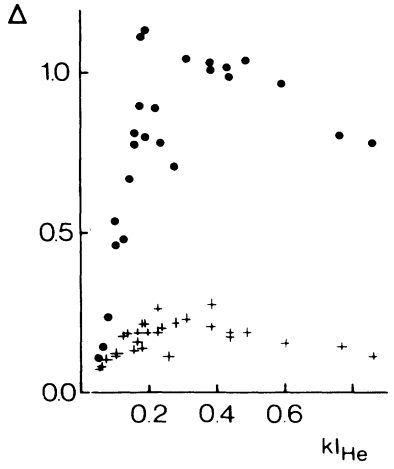

FIG. 3. Comparison of the shifts and widths the Brillouin lines before and after the correction for the asymmetric contribution to the Brillouin lines. The ratio $(\omega_{corr}-\omega_{uncorr})/\omega_{uncorr}$ is plotted as a function of kl_{He} (density-dependent experiments). He+Xe mixture, $T=294$ K, $x_{Xe}=0.45$. Dots, width of the Brillouin lines; crosses, Brillouin shift.

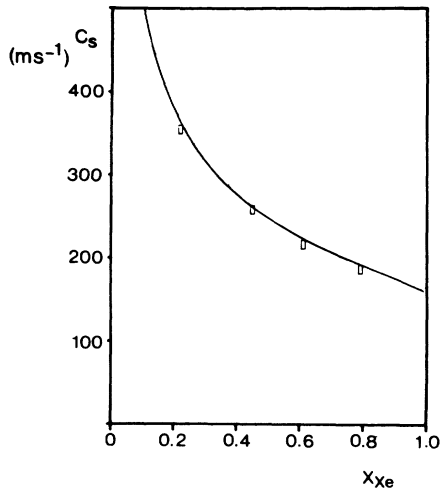

FIG. 4. Sound velocity as a function of the xenon mole fraction for various He+Xe mixtures at a pressure $p\cong 38.9$ bar. The rectangles are experimental results: $c_s=\omega/k$. The drawn line represents the result of c_s calculated with the equation of state.

of magnitude, then we find that the value of z_{D+} draws near to z_{D-}. Therefore, one may conclude that the representation of the Rayleigh line by a single Lorentzian is a reasonable assumption. More detailed information concerning the Rayleigh line can only be obtained using light-beating spectroscopy.

In Fig. 3 we illustrate the influence of the asymmetric contribution to the Brillouin lines on the shifts and widths, as obtained from two series of density-dependent measurements ($x_{Xe}=0.61$ and $x_{Xe}=0.45$). As can be seen from Fig. 3, the fitting procedure with only

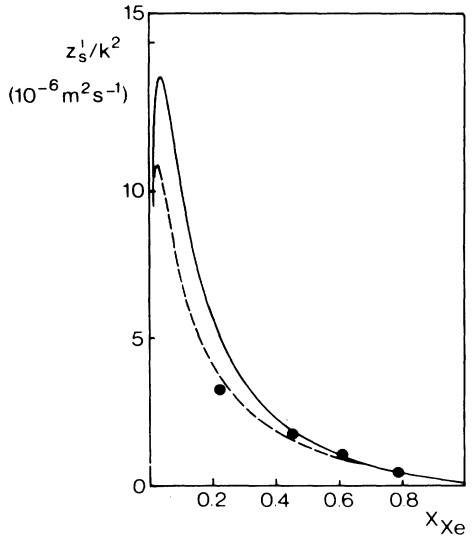

FIG. 5. The normalized attenuation factor z_s'/k^2 as a function of the xenon mole fraction for various He+Xe mixtures at a pressure $p\cong 38.9$ bar. The rectangles are experimental results. The drawn line represents the result of z_s'/k^2 calculated with Eq. (2.13). The dashed line represents the ideal gas limit.

Lorentzians yields values for the Brillouin shift which are approximately 2–20 % smaller than those values which are found when the asymmetric term is taken into consideration. For the width of the Brillouin lines the difference between the results of the two fitting procedures is more drastic. The derived width can become 80% larger when the asymmetric contribution is taken into account. Unless stated otherwise we will show throughout the remainder of this article the attenuation factor z_s' and the propagation frequency of the second mode z_s'' (i.e., the real and imaginary parts of the eigenvalue z_s). They are the width and the shift of the Brillouin lines corrected for the asymmetric term and therefore the "true" propagation frequency and attenuation of the second mode.

At a total pressure of 39 bar the Brillouin lines are well separated from the Rayleigh line for most compositions ($x_{Xe} > 0.3$). The wave-vector dependence of the sound-propagation frequency derived from the Brillouin shift conforms to a straight line at this relatively high pressure.[13] The composition dependence of the propagation frequency and the attenuation factor at a pressure of 39 bar is shown in Figs. 4 and 5. The solid lines are results of the thermodynamic and hydrodynamic calculations presented in a previous publication.[6] In the calculations we used input parameters which are based on experimentally determined virial and transport coefficients (see Refs. 6, 13, and 22). There are no adjustable parameters. From the calculations we deduce that the value for the attenuation factor z_s' in the small wave-vector limit is largely determined by the last term of Eq. (2.4): $(\rho c_s \mathcal{P})^2 (\partial\mu/\partial c)_{p,T} D$. In this term the osmotic compressibility $(\partial\mu/\partial c)_{p,T}$ is very sensitive to small variations in the virial coefficients used to calculate this quantity. This can be inferred from the difference between the values calculated with the virial equation of state and the ideal gas values which are represented as the dashed line in Fig. 5. The discrepancy observed between the calculated and experimental value at $x_{Xe} = 0.22$ has to be attributed to an incorrect value for the virial coefficients. Rather then to adjust the value to fit the data we used the experimental value for the virial coefficient for all calculations, since at lower densities the discrepancy becomes negligible. It is in the low-density region that the interesting phenomena are observed. Notwithstanding the differences the experimental results give evidence of the validity of the small wave-vector limit at 39 bar.

As the pressure is lowered the Rayleigh and the Brillouin lines broaden significantly,[13] while the propagation frequency tends towards values smaller than $c_s k$. In Fig. 6 the wave-vector dependence of the propagation frequency and the attenuation factor of the sound mode is shown for a He+Xe mixture with a pressure of 9.9 bar and $x_{Xe} = 0.53 \pm 0.02$.[13] The experimental results are

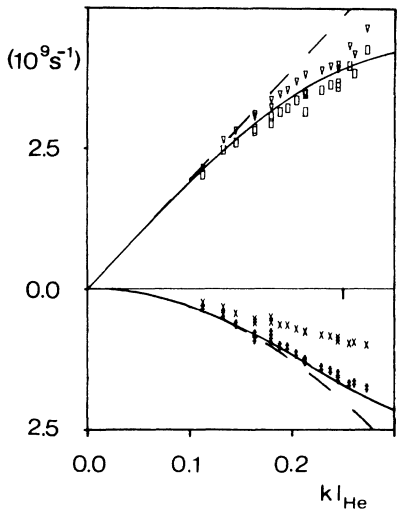

FIG. 6. Brillouin shift $\omega(k)$ and the width of the Brillouin lines $\Gamma(k)$ for the He+Xe mixture with $x_{Xe} = 0.53 \pm 0.02$ and $p = 9.9$ bar as a function of the wave vector. The drawn line represent the results of a hydrodynamic calculation for $x_{Xe} = 0.53$. The dashed lines represent the small wave-vector limit of the hydrodynamic theory. The vertical bar indicates the half-width at half maximum of the instrumental profile. □, Brillouin shift, not corrected for the asymmetric contribution; ∇, Brillouin shift corrected for the asymmetric contribution, using Fig. 3; ×, Brillouin width, not corrected for the asymmetric contribution; #, Brillouin width corrected for the asymmetric contribution, using Fig. 3.

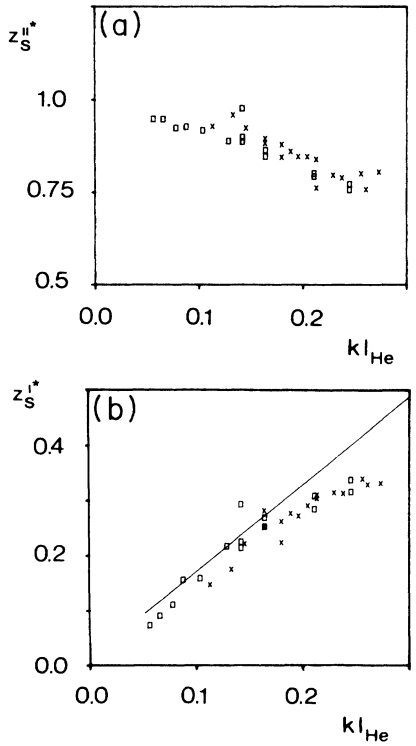

FIG. 7. A comparison between wave-vector-dependent (crosses) and density-dependent experiments (squares) on the He+Xe mixture with $x_{He} = 0.53 \pm 0.02$, as a function of the reduced wave vector kl_{He}. (a) The reduced propagation frequency $(z_s'')^* = z_s''/c_s k$; (b) the reduced attenuation factor $(z_s')^* = z_s'/c_s k$. The results of the wave-vector-dependent experiments are also shown in Fig. 6. The drawn line represents the small wave-vector limit.

compared with the results of a (wave-vector-dependent) hydrodynamic calculation for a mixture with $x_{Xe}=0.53$. It can be seen that a linear dispersion is no longer sufficient to describe the wave-vector dependence of the propagation frequency. Similarly, the attenuation factor deviates from the kl_{He} dependence in the small wave-vector limit. The experimental results agree qualitatively with the hydrodynamic predictions.

In a previous paper,[6] we have shown that the reduced eigenvalues of the hydrodynamic matrix $z^*=z/(c_s k)$ are proportional to k/ρ as long as the ideal-gas approximation is valid. Thus it is possible to obtain dispersion relations by plotting the reduced propagation frequencies and attenuation factors as a function of the reduced wave vector kl_{He}, where kl_{He} is varied by changing the density. But for the experimental convenience, this method has the advantage that a larger kl_{He} domain is accessible than when the scattering angle is varied. An experimental comparison between the two methods, for a He+Xe mixture with $x_{Xe}=0.53\pm0.02$, is given in Fig. 7. We have used here the data also shown in Fig. 6 ($p=9.9$ bar; k ranges from 9.2×10^6 m^{-1} to 2.22×10^7 m^{-1}), together with data from experiments in which the pressure of the mixture varied from 41.8 bar to 9.9 bar ($k=1.99\times10^7$ m^{-1}).[13] Although the reduced propagation frequencies obtained in the density-dependent experiments tend to fall somewhat below the shifts which were measured while k was varied, it is clear that $z^*(k)$ does scale with kl_{He}.

In the next part of this paper, we present the results of the density-dependent experiments. The reduced wave-vector dependence of the reduced propagation frequency $(z_s'')^*=z_s''/(c_s k)$ is shown in Fig. 8. For the mixtures considered here the $(z_s'')^*$ becomes smaller as kl_{He} increases. The reduction of the propagation frequency becomes more pronounced as the xenon mole fraction decreases. Comparing the reduced propagation frequency with the prediction of density-dependent hydrodynamic calculations, one finds for reduced wave vectors up to $kl_{He}=0.25$, a reasonable correspondence between theory and experiment. However, the hydrodynamic theory overestimates the damping of the sound mode as kl_{He} becomes larger than 0.3. For large kl_{He} the shift tends towards the ideal gas value $c_s k$ of pure xenon. This is the manifestation of a "slow" sound mode.[20] For a mole fraction $x_{Xe}=0.45$, one finds for small values of kl_{He} the experimental points above the theoretical curve. This is again due to an incorrect value of the virial coefficients as pointed out above at Fig. 5.

In Fig. 9, we compare the experimental results concerning the reduced sound mode attenuation factor $(z_s')^*=z_s'/c_s k$ with the calculated value of $(z_s')^*$. For small reduced wave vectors we find that the reduced attenuation factor increases linearly with kl_{He}, in agreement with the prediction in the small wave-vector limit of the hydrodynamic theory. For mixtures with $x_{Xe}=0.61$ and $x_{Xe}=0.45$ a quantitative agreement is found with the theoretical predictions for small kl_{He}. For the mixture with $x_{Xe}=0.22$ in the same kl_{He} region we find only a qualitative agreement. The kl_{He} dependence of the re-

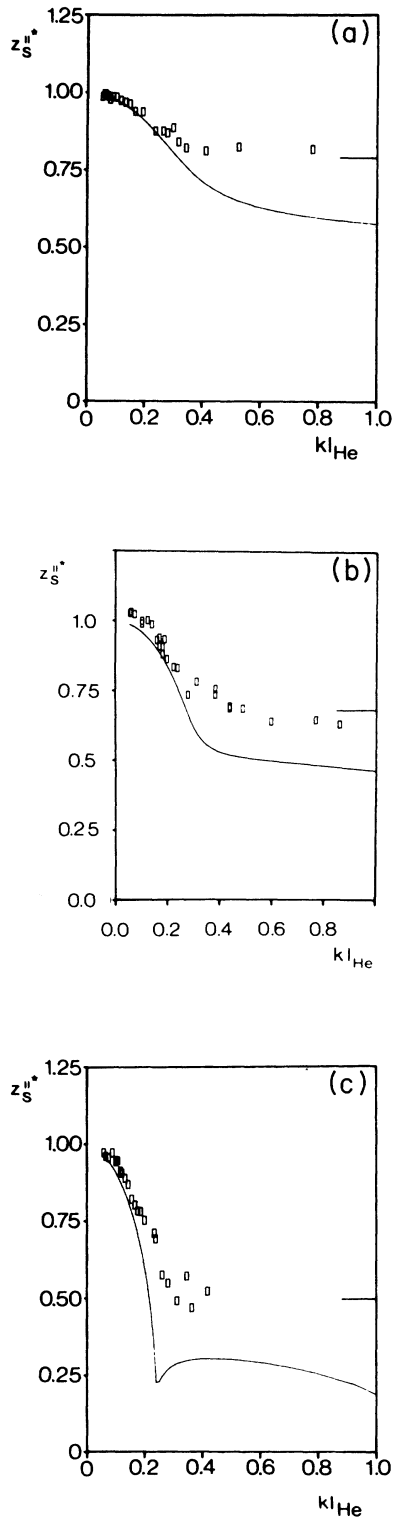

FIG. 8. Reduced propagation frequency as a function of the reduced wave vector. The squares are our experimental results. The drawn line represents the result of a density-dependent hydrodynamic calculation of z_s''. The horizontal bar represents the value of the ratio $c_s(\mathrm{Xe})/c_s$ (mixture). (a) $x_{Xe}=0.61$; (b) $x_{Xe}=0.4$; (c) $x_{Xe}=0.22$.

duced attenuation factor of the sound mode undergoes a change in slope in the region $0.2 \leq kl_{He} \leq 0.3$. This change, which can be observed both in the experimental and calculated results, becomes more pronounced as the xenon mole fraction decreases. However, in the case of the mixtures with $x_{Xe}=0.45$ and $x_{Xe}=0.22$, the reduced wave vector at which this change takes place seems to coincide with the kl_{He} value at which the hydrodynamic description starts to deviate from the experimental results.

In Fig. 2 is illustrated that the light scattering spectra can become rather featureless when kl_{He} exceeds 0.15. As a result the spectra are difficult to analyze and this gives rise to an uncertainty in the parameters which are extracted from the experiments. However, the function $\omega^2 I(k,\omega)$ can be analyzed easily for all reduced wave vectors. In Fig. 10 we show a few examples of $\omega^2 I(k,\omega)$ of the He+Xe mixture with $x_{Xe}=0.22$. The baseline is estimated by averaging over a number of points on the borders of successive orders of the interferogram. The reduced peak positions $\omega_m^*(k)=\omega_m(k)/c_s k$ of $\omega^2 I(k,\omega)$ the mixtures with $x_{Xe}=0.79$, $x_{Xe}=0.61$, $x_{Xe}=0.45$, $x_{Xe}=0.38$, and $x_{Xe}=0.22$, are shown in Fig. 11 plotted as a function of the reduced wave vector kl_{He}. The hydrodynamic calculation of $z_s''^*$ predicts the peak positions of $\omega^2 I(k,\omega)$ well up to $kl_{He} \cong 0.2$. For all the measured dispersion relations of $\omega_m^*(k)$ a significant deviation from the calculated dispersion is obtained when kl_{He} exceeds 0.3. It can be seen that when the dispersion relation deviates from the hydrodynamic values it tends towards the values of the Gaussian limit, $v_{Xe}\sqrt{2}/c_s$, which is larger than the calculated value of $(z_s'')^*$.

Summarizing the results, we have concluded on the basis of ample experimental evidence that the reduced propagation frequency and reduced attenuation factor are to a good approximation a function of the quotient of the wave vector and the density only. We applied this observed scaling behavior by presenting the results of wave-vector-dependent experiments as well as density-dependent experiments as a function of the reduced wave vector kl_{He}. In this way we are able to measure dispersion relations over a range of kl_{He} values that is not accessible by experiments in which only the scattering angle is varied. We have found that a transition from hydrodynamic to kinetic behavior occurs for the reduced wave vectors $0.18 < kl_{He} < 0.3$. The same transition is found in the reduced wave-vector dependence of the peak positions of $\omega^2 I(k,\omega)$. This function appears to be extremely useful when the light-scattering spectrum becomes featureless. Finally, for large reduced wave vectors we have found that the sound-propagation frequency tends

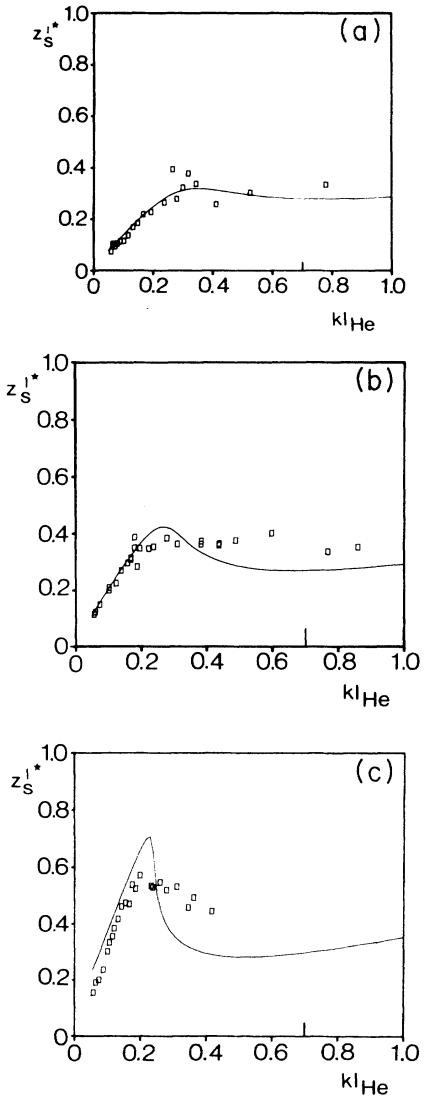

FIG. 9. Reduced sound-mode attenuation factor as a function of the reduced wave vector. The squares are our experimental results. The drawn line represents the result of a density-dependent hydrodynamic calculation of z_s'. The vertical bar indicates the reduced half-width at half maximum of the instrumental profile. (a) $x_{Xe}=0.61$; (b) $x_{Xe}=0.45$; (c) $x_{Xe}=0.22$.

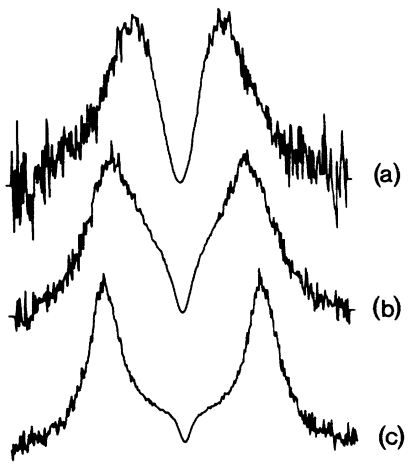

FIG. 10. Several examples $\omega^2 I(k,\omega)$. Thermodynamic circumstances: $x_{Xe}=0.22$, $T=294$ K. Curve a, $p=6.4$ bar, $kl_{He}=0.35$; curve b, $p=18.3$ bar, $kl_{He}=0.12$; curve c, $p=38.7$ bar, $kl_{He}=0.06$. The corresponding line shapes $I(k,\omega)$ are shown in Fig. 2(b).

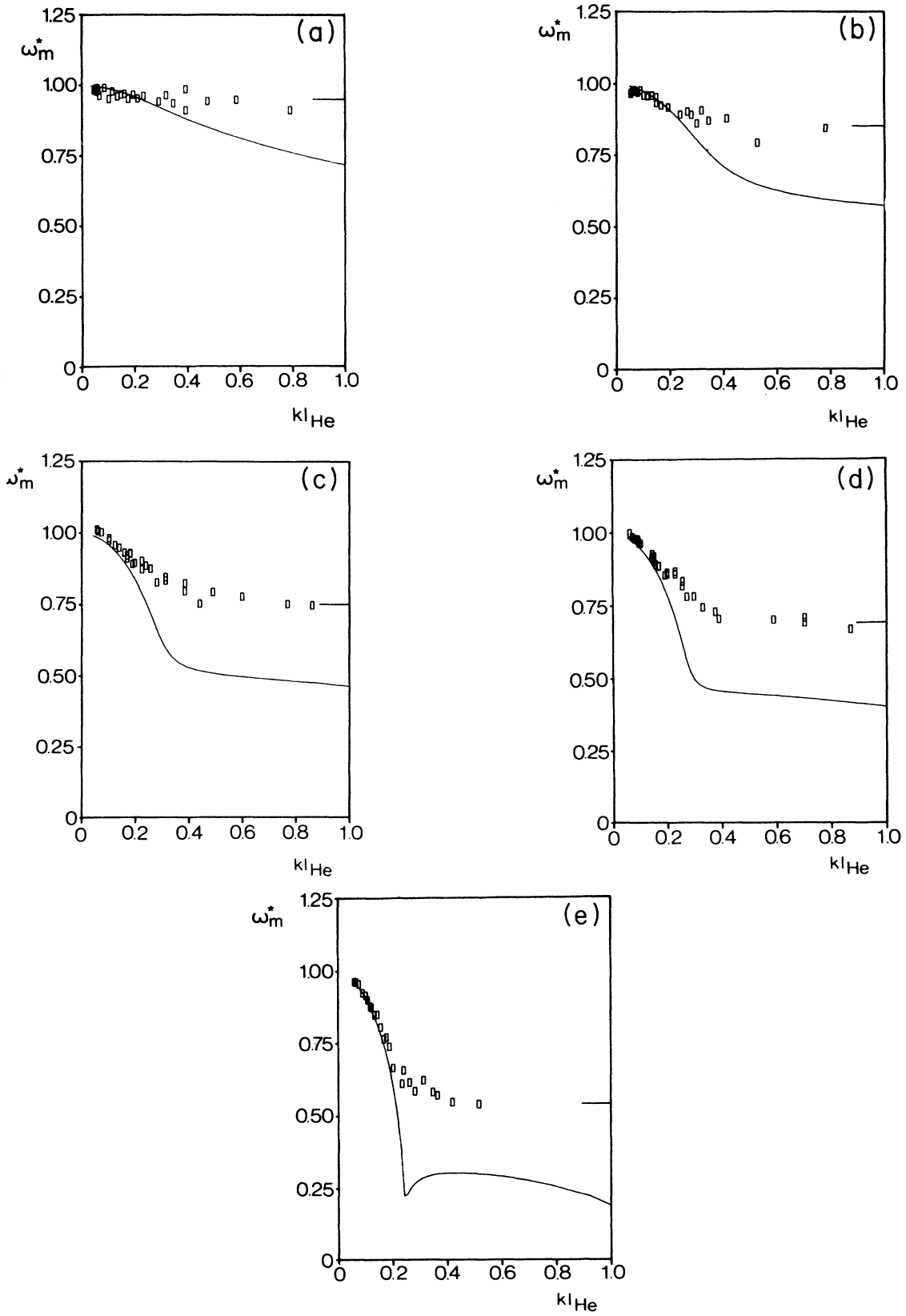

FIG. 11. Reduced peak positions of $\omega^2 I(k,\omega)$ as a function of the reduced wave vector for several He+Xe mixtures. The squares are our experimental results. The drawn line represents the result of a hydrodynamic calculation of $\mathrm{Im}z_s$. The horizontal bar indicates the Gaussian limit. (a) $x_{Xe}=0.79$; (b) $x_{Xe}=0.61$; (c) $x_{Xe}=0.45$; (d) $x_{Xe}=0.38$; (e) $x_{Xe}=0.22$.

towards the value of $c_s k$ of pure xenon. This is the slow sound mode which is supported by the xenon density fluctuations.

V. DISCUSSION

In this paper we studied the density and wave-vector dependence of the Rayleigh-Brillouin spectrum of binary noble gas mixtures consisting of components with a large disparity in mass. We found that the dispersion of the sound wave may, under certain circumstances, deviate from the linear dispersion law $z_s''=c_s/k$. These deviations from the small wave-vector limit become more apparent as the concentration of the lighter component of the gas gets larger. A review of the location in the kl_{He}-x_{Xe} plane of our density-dependent measurements (represented by squares) is given in Fig. 12, together with the composition dependence of three features that are predicted by the hydrodynamic theory. The black areas in Fig. 12 designate the predicted location of the sound propagation gaps in the kl_{He}-x_{Xe} plane.[6] For He+Xe gas mixtures with $x_{\mathrm{Xe}}<0.45$ the theory predicts a value for the reduced wave vector kl_{He} for which the "group velocity" dz_s''/dk becomes equal to zero.[6] These values of kl_{He} are represented in Fig. 12 by line I. Also shown in Fig. 12 are the kl_{He} values for which the amplitude of the Brillouin line is predicted to become larger than the amplitude of the Rayleigh line. The composition dependence of these kl_{He} values is given by line II. On the basis of our experimental results, we are able to determine the range of kl_{He} values for which the hydrodynamic theory is valid. From Fig. 11 it can be deduced that the hydrodynamic description of the peak positions of $\omega^2 I(k,\omega)$ ceases to be valid when kl_{He} exceeds $kl_{\mathrm{He}}\cong 0.2$. These particular values are represented in Fig. 12 by a big, black dot. The reduced wave-vector dependence of

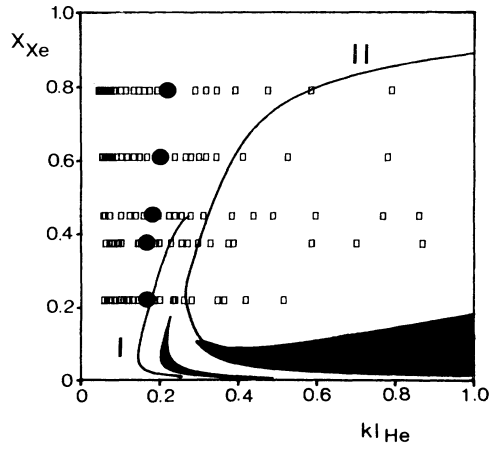

FIG. 12. Comparison of the location of our measurements in the kl_{He}-x_{Xe} plane (squares), and the location of the phenomena predicted by the hydrodynamic theory. The black dot represents the kl_{He}-x_{Xe} value at which we have observed the first deviation from the hydrodynamic theory. Black area, no propagating modes; line I, zero group velocity $d\mathrm{Im}z_s/dk=0$; line II, the amplitude of the Brillouin line equals the amplitude of the Rayleigh line.

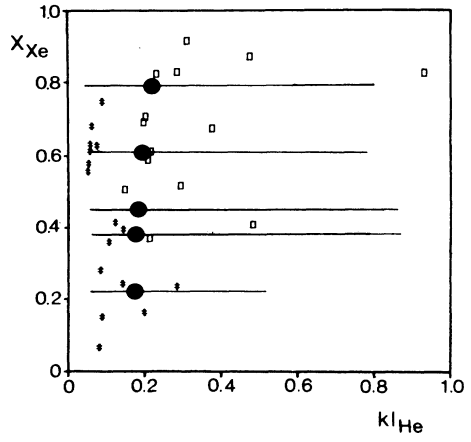

FIG. 13. Comparison between our experimental results (horizontal lines) and those of Letamendia *et al.* (Ref. 5). The black dot represents the kl_{He}-x_{Xe} value at which we have observed the first deviation from the hydrodynamic theory. #, Letamendia *et al.*, hydrodynamic line shape (*H*); □, Letamendia *et al.*, nonhydrodynamic line shape (NH). (See also Fig. 12.)

the various quantities that we have obtained from the spectral line shape $I(k,\omega)$ also support the suggestion that the hydrodynamic theory is valid up to $kl_{\mathrm{He}}\cong 0.2\pm 0.07$. This value of kl_{He} appears to be independent of the composition, and is considerably smaller than the kl_{He} value at which the Rayleigh line and the Brillouin lines are predicted to have equal amplitudes (line II in Fig. 12).

Shown in Fig. 13 are the (kl_{He},x_{Xe}) values for which Letamendia *et al.*[5] have measured Rayleigh-Brillouin spectra. The squares represent the measurements for which they found the line shape in accordance with the hydrodynamic theory, while the crosses represent the measurements which could not be explained by the hydrodynamic theory. From Fig. 13 it can be seen that a good correspondence is obtained between our results and those of Letamendia *et al.*,[5] except for mixtures with $x_{\mathrm{Xe}}<0.25$.

In liquid noble gases, an anomalous deviation from linear positive dispersion has been found due to mode coupling.[14(a),25] Our measurements do not indicate similar effects to occur in low-density gas mixtures.

In one-component gases no dramatic change in the wave-vector dependence of the dispersion curve can be observed as the wave vector changes from $kl\ll 1$ to $kl=O(1)$.[4] This prediction is more or less confirmed by our finding that the deivations of linear dispersion become smaller as the xenon concentration increases. For large reduced wave vectors, the measurements indicate that the shift of the Brillouin lines tends towards the value of $z_s''(k)=c_s k$ of pure xenon.

In this context we mention the computer simulations of a Li+Pb mixture performed by Bosse *et al.*[18] and the calculations of Campa and Cohen.[19] Their results indicate that for sufficiently large wave vectors propagating waves in the density of the heavy particles, and propagating waves which are supported by the light particles (fast sound), are present. Up to this moment most attention

has been paid to the fast sound mode.[18–20] Such a propagating fast sound mode cannot be measured by light scattering in the He+Xe gas mixture, since helium scatters light very poorly.[19,22] Our experiments have revealed that for large wave vectors a slow sound wave is present which is supported by the heavy particles (i.e., xenon).

In a previous paper we have used the concept of two propagating modes in order to present a simple, intuitive model which provides us with an idea why the sound modes are significantly damped when $x_{Xe} > 0.5$. This model predicts the existence of a intermediate composition region $0.15 \leq x_{Xe} \leq 0.5$ in which neither the fluctuations in the xenon density not the fluctuations in the helium density dominate the dynamics of the mixture. This agrees with the prediction by Bowler and Johnson who predict one "critical composition" for sound propagation at around $x_{Xe} \cong 0.5$.[26]

In Ref. 6 we used kinetic arguments to show that the damping of the eigenmodes must be attributed to a transition from a system dominated by heavy particles to a system dominated by light particles. The concept of such a transition is also supported by thermodynamic arguments. In Ref. 6 we have shown that the composition dependence of $(\partial\mu/\partial c)^{-1}_{p,T}$ has a sharp peaked extremum around $x_{Xe} \cong 0.02$. Since μ is the first-order derivative of the Gibbs free energy, one may conclude that the transition we are dealing with is analogous to a continuous phase transition.[27] It should be remembered that $(\partial\mu/\partial c)_{p,T}$ is one of the quantities which, to a large extent, determine the shape of the sound dispersion curve.[6]

ACKNOWLEDGMENTS

We gratefully acknowledge the discussions we have had with Dr. I. M. de Schepper and Professor J. van der Elsken. This work is part of the research program of the foundation for Fundamental Research of Matter (FOM), supported by the Netherlands foundation for Chemical Research (SON) and was made possible by financial support from the Netherlands Organization for Scientific Research.

[1] B. Berne and R. Pecora, *Dynamic Light Scattering* (Wiley, New York, 1976).
[2] J. P. Boon and S. Yip, *Molecular Hydrodynamics* (McGraw-Hill, New York, 1980).
[3] W. Hayes and R. Loudon, *Scattering of Light by Crystals* (Wiley, New York, 1978).
[4] B. Kamgar-Parsi, E. G. D. Cohen, and I. M. de Schepper, Phys. Rev. A **35**, 4781 (1987).
[5] L. Letamendia, J.-P. Chabrat, G. Nouchi, J. Rouch, C. Vaucamps, and S.-H. Chen, Phys. Rev. A **24**, 1574 (1978).
[6] G. H. Wegdam and H. M. Schaink, Mol. Phys. **65**, 531 (1988).
[7] W. S. Gornall, C. S. Wang, C. C. Yang, and N. Bloembergen, Phys. Rev. Lett. **26**, 1094 (1971).
[8] N. A. Clark, Phys. Rev. A **12**, 2092 (1975).
[9] Q. H. Lao, P. E. Schoen, B. Chu, and D. A. Jackson, J. Chem. Phys. **64**, 5013 (1976).
[10] W. S. Gornall and C. S. Wang, J. Phys. (Paris) Colloq. Suppl. 2-3, C1-33 51 (1972).
[11] B. Y. Baharudin, P. E. Schoen, and D. A. Jackson, Phys. Lett. **42A**, 77 (1972).
[12] H. N. W. Lekkerkerker and J. P. Boon, Phys. Lett. **39A**, 9 (1972).
[13] H. M. Schaink and G. H. Wegdam, Physica **141A**, 211 (1987); Physica A **160**, 117 (1989).
[14] (a) I. M. de Schepper, P. Verkerk, A. A. van Well, and L. A. de Graaf, Phys. Rev. Lett. **50**, 974 (1983); (b) A. A. van Well, P. Verkerk, L. A. de Graaf, J.-B. Suck, and J. R. D. Copley, Phys. Rev. A **31**, 3391 (1985).
[15] J. R. D. Copley and J. M. Rowe, Phys. Rev. Lett. **32**, 49 (1974).
[16] J. B. Suck, H. Rudin, H. J. Güntherodt, and H. Beck, Phys. Rev. Lett. **50**, 49 (1983).
[17] R. L. McGreevy and E. W. Mitchell, J. Phys. C **18**, 1163 (1985).
[18] J. Bosse, G. Jacucci, M. Ronchetti, and W. Schirmacher, Phys. Rev. Lett. **57**, 3277 (1986).
[19] (a) A. Campa and E. G. D. Cohen, Phys. Rev. Lett. **61**, 853 (1988); (b) Phys. Rev. A **39**, 4904 (1989).
[20] W. Montfrooij, P. Westerhuijs, V. O. de Haan, and I. M. de Schepper, Phys. Rev. Lett. **63**, 544 (1989); Results of preliminary calculations can be found in W. Montfrooij, P. Westerhuijs, and I. M. de Schepper, Phys. Rev. Lett. **61**, 2155 (1988).
[21] C. Cohen, J. W. H. Sutherland, and J. M. Deutch, Phys. Chem. Liq. **2**, 213 (1971).
[22] H. M. Schaink, Ph.D. thesis, University of Amsterdam, 1989.
[23] R. C. Burns, C. Graham, and A. R. M. Weller, Mol. Phys. **59**, 41 (1986).
[24] J. O. Hirschfelder, C. F. Curtis, and R. B. Bird, *Molecular Theory of Gases and Liquids* (Wiley, New York, 1964).
[25] I. M. de Schepper, P. Verkerk, A. A. van Well, and L. A. de Graaf, Phys. Lett. **104A**, 29 (1984).
[26] (a) J. R. Bowler and E. A. Johnson, Phys. Rev. Lett. **54**, 329 (1985); (b) Proc. R. Soc. London Ser. A **408**, 79 (1986).
[27] L. E. Reichl, *A Modern Course in Statistical Physics* (Edward Arnold, London, 1980).